Deviations from unity of the ratio of the turbulent Schmidt to Prandtl numbers in stratified atmospheric flows over water surfaces

Gabriel G. Katul,[1,2,*] Dan Li,[3] Heping Liu,[4] and Shmuel Assouline[5]

[1]*Nicholas School of the Environment, Box 80328, Duke University, Durham, North Carolina 27708, USA*

[2]*Department of Civil and Environmental Engineering, Duke University, Durham, North Carolina 27708, USA*

[3]*Department of Earth and Environment, Boston University, Boston, Massachusetts 02215, USA*

[4]*Department of Civil and Environmental Engineering, Post Office Box 642910, Washington State University, Pullman, Washington 99164-2910, USA*

[5]*Department of Environmental Physics and Irrigation Institute of Soils, Water and Environment Sciences, Agricultural Research Organization, Volcani Center, Post Office Box 6, Bet Dagan 50250, Israel*

(Received 12 April 2016; published 20 July 2016)

Expressions for the ratio of the turbulent Schmidt (Sc_t) to Prandtl (Pr_t) numbers are derived for an idealized atmospheric surface layer flow over water surfaces. Conditions where the ansatz $\mathrm{Sc}_t/\mathrm{Pr}_t \approx 1$ are then discussed. It is shown that $\mathrm{Sc}_t/\mathrm{Pr}_t \approx 1$ is consistent with the active role of temperature in turbulence generation or destruction even when perfect similarity between turbulent transport of heat and water vapor is absent.

DOI: 10.1103/PhysRevFluids.1.034401

I. INTRODUCTION

Despite their ad hoc introduction some 140 years ago [1], eddy diffusivity and eddy viscosity (K_m) remain fruitful concepts in turbulence research. They qualify as the first successful application of renormalization group (RNG) methods, arguably well before RNG's formal development in quantum field theory [2]. Their use has made it possible to measure and model turbulent fluxes in natural systems operating at Reynolds numbers that are simply too large to resolve in direct numerical simulations. A case in point is the 1926 seminal work of the physicist Ira Bowen [3,4], who determined lake evaporation (E) and heat conduction (H) using the concept of eddy diffusivity and similarity between heat and water vapor transport. Bowen's original derivation assumed the ratio of eddy diffusivity for heat (K_T) to water vapor (K_q) or equivalently the ratio of the turbulent Schmidt ($\mathrm{Sc}_t = K_m/K_q$) to Prandtl ($\mathrm{Pr}_t = K_m/K_T$) numbers be unity. This assumption is now routinely employed in climate and weather forecasting models [5,6] and is justified using similarity in heat and water vapor sources and sinks at the water surface along with similarity in turbulent transport characteristics [7]. There is renewed interest in deviations from unity in $\mathrm{Sc}_t/\mathrm{Pr}_t$ given the proliferation of remote-sensing products aimed at inferring the Bowen ratio $\beta = H/E$ from radiometric mean surface (T_s) measurements [8–13]. This inference of β from T_s and theoretical limits on β at a given T_s routinely assumes $\mathrm{Sc}_t/\mathrm{Pr}_t = 1$ [14–18] as in the original work of Bowen.

To be clear, this assumption cannot be entirely correct [19–22] as temperature is an active scalar (i.e., a scalar that produces or dissipates turbulent kinetic energy). Water vapor concentration turbulent fluctuations also impact air density, though this impact is usually small when compared to their temperature counterparts. Measurements of the correlation coefficient between turbulent air temperature and water vapor concentration fluctuations R_{Tq} above large water bodies also challenge the assumption $\mathrm{Sc}_t/\mathrm{Pr}_t = 1$. The R_{Tq} is used as a so-called signature of scalar similarity but deviations from unity are routinely reported [22–24]. Over land, it has been known for some time that K_T and K_q can differ and the difference partly depends on the thermal stratification in the atmosphere [25,26]. Moreover, in the presence of horizontal advection or entrainment, K_T and K_q also differ [27–32] with some experiments reporting $K_T/K_q > 5$ [33]. Nonetheless, the weighty Kansas experiment over flat and uniform surface [34] suggests that $K_T \approx K_q$ across a wide range of

*Corresponding author: gaby@duke.edu

atmospheric stability regimes [35], which was also confirmed by other extensive experiments [36]. Studies over large water bodies also appear mixed with regards to $K_T = K_q$ when analyzed in the context of R_{Tq}. Some experiments favor near-perfect similarity [37] while others report nontrivial deviations from unity [38,39] in $|R_{Tq}|$. Likewise, deviations in $|R_{Tq}|$ from unity over oceans have also been reported in several large-scale experiments [40]. The reason why R_{Tq} deviates from unity near the surface, even in the absence of horizontal advection, is partly connected with scalar dissimilarity in entrainment at the top of the atmospheric boundary layer, as confirmed by a large corpus of experiments and simulations [24,30,31,41,42]. The apparent contradiction in setting $K_T/K_q \approx 1$ despite $|R_{Tq}| < 1$ and the fact that air temperature is an active scalar are examined here. The goal is to explain maximum deviations in K_T/K_q from unity due to these two aforementioned effects. Advection, subsidence, and nonstationary conditions are not considered as they act above and beyond these cases. Advective conditions, which are prevalent in some experiments [27–29,33,43], are more difficult to discuss because turbulent fluxes are no longer constant with height z and the advective time scale may be comparable with the equilibration time scale, raising questions as to whether gradient-diffusion closure (or K theory) applies [44,45].

II. THEORY

A. Definitions

The idealized setup by Bowen is first considered [3,4]. This setup assumes a stationary and planar-homogeneous high Reynolds number air flow at some height z over a uniform water surface in the absence of any subsidence. The net available energy Q_n at the air-water interface is partitioned into sensible H and latent E heat fluxes so that $Q_n = E + H$. By definition [3,4], $\beta = H/E$ and $E = Q_n(1+\beta)^{-1}$. It is further assumed that $\beta \neq -1$ and $|E| > 0$. If molecular diffusion coefficients for heat and water vapor in air are ignored relative to their turbulent counterparts (K_T and K_q), then the actual evaporation is given by the turbulent flux $E = L_v\overline{w'q'}$ and the sensible heat flux is given by $H = \rho C_p \overline{w'T'}$, where L_v is the latent heat of vaporization, ρ is the mean air density, C_p is the specific heat capacity of dry air at constant pressure, w' is the turbulent vertical velocity excursion from the mean state $\overline{w} = 0$ (no subsidence), T' and q' are turbulent air temperature and water vapor concentration excursions from their mean $\overline{T}(z)$ and $\overline{q}(z)$, and an overline indicates Reynolds averaging. Using K theory, the turbulent scalar fluxes are given by

$$\overline{w'q'} = -K_q \frac{d\overline{q}}{dz}; \quad \overline{w'T'} = -K_T \frac{d\overline{T}}{dz}. \tag{1}$$

Likewise, the kinematic turbulent stress is given by

$$\frac{\tau_t}{\rho} = -\overline{w'u'} = u_*^2 = K_m \frac{d\overline{U}}{dz}, \tag{2}$$

where u' are turbulent excursions from the mean longitudinal velocity $\overline{U}$, $\overline{w'u'}$ is the turbulent momentum flux, K_m is assumed to be much larger than the molecular viscosity of air ν, and u_* is the friction or shear velocity. Throughout, the Reynolds number $\mathrm{Re}_* = u_* z/\nu$ is assumed to be sufficiently large to ignore viscous effects. This assumption is plausible in the atmospheric surface layer (ASL) over water surfaces, where $u_* \sim 0.1$ m s^{-1}, $z \sim 1$ m, and $\nu \sim 1.5 \times 10^{-5}$ m^2 s^{-1}. Exploring how K_T/K_q varies for such idealized flow is equivalent to evaluating how $\mathrm{Sc}_t/\mathrm{Pr}_t$ varies with atmospheric stability and other bulk flow variables (e.g., boundary layer height).

As is conventional in the analysis of ASL flows, dimensionless quantities for the first and second moments are considered and are defined as [46,47]

$$\frac{d\overline{T}}{dz} = \frac{T_*}{\kappa z}\phi_h(\varsigma); \quad \frac{d\overline{q}}{dz} = \frac{q_*}{\kappa z}\phi_v(\varsigma); \quad \frac{d\overline{U}}{dz} = \frac{u_*}{\kappa z}\phi_m(\varsigma); \tag{3}$$

$$\frac{\sigma_w}{u_*} = \phi_{ww}(\varsigma); \quad \frac{\sigma_T}{T_*} = \phi_{TT}(\varsigma); \quad \frac{\sigma_q}{q_*} = \phi_{qq}(\varsigma); \tag{4}$$

where ϕ_h, ϕ_v, and ϕ_m are referred to as stability correction functions for heat, water vapor, and momentum, respectively; $\sigma_T^2 = \overline{T'T'}$; $\sigma_q^2 = \overline{q'q'}$; $\sigma_w^2 = \overline{w'w'}$; and T_*, q_*, the stability parameter ς, and the Obukhov length L [48] are, respectively, given as

$$T_* = -\frac{\overline{w'T'}}{u_*}; \quad q_* = -\frac{\overline{w'q'}}{u_*}; \quad \varsigma = \frac{z}{L}; \quad L = \frac{u_*^2}{\kappa\beta_o T_*}, \tag{5}$$

where $\kappa \approx 0.4$ is the von Kármán constant, $\beta_o = g/T_a$ is the buoyancy parameter, and $g = 9.81$ m s^{-2} is the gravitational acceleration. Here, unstable, stable, and near-neutral atmospheric stability conditions are associated with $\varsigma < 0$, $\varsigma > 0$, and $\varsigma \approx 0$, respectively. A $\varsigma \approx -1$ signifies a height at which mechanical production of turbulent kinetic energy (TKE) is commensurate with buoyant production of TKE. In the definition of L, it was assumed that water vapor concentration corrections are small relative to their temperature counterpart. Based on these definitions,

$$\frac{K_T}{K_q} = \frac{\mathrm{Sc}_t}{\mathrm{Pr}_t} = \frac{\phi_v(\varsigma)}{\phi_h(\varsigma)}. \tag{6}$$

To illustrate the utility of K_T/K_q to the plethora of problems earlier mentioned, it is noted that

$$\left(\frac{K_T}{K_q}\right)\frac{\frac{d\overline{T}}{dz}}{\frac{d\overline{q}}{dz}} = \frac{\sigma_w\sigma_T R_{wT}}{\sigma_w\sigma_q R_{wq}}, \tag{7}$$

which when combined with the similarity theory expressions yields

$$\frac{\phi_{TT}(\varsigma)}{\phi_{qq}(\varsigma)} = \left(\frac{R_{wT}}{R_{wq}}\right)^{-1}. \tag{8}$$

The quantity R_{wT}/R_{wq} is labeled as the relative transport efficiency of heat to water vapor [22,49]. With these expressions,

$$\beta = \frac{H}{E} = \frac{\rho C_p}{L_v}\left(\frac{K_T}{K_q}\right)\frac{\frac{d\overline{T}}{dz}}{\frac{d\overline{q}}{dz}} = \beta_{ap}\left(\frac{K_T}{K_q}\right), \tag{9}$$

where

$$\beta_{ap} \approx \frac{\rho C_p}{L_v}\frac{\overline{T_s} - \overline{T}(z)}{q(\overline{T_s}) - \overline{q}(z)}, \tag{10}$$

is mainly used to link remotely sensed $\overline{T_s}$ to β given that the (saturated) water vapor concentration at the water surface $q(\overline{T_s})$ can be predicted from T_s using the Clausius-Clapeyron expression. As earlier noted, if similarity of heat and water vapor transport is invoked, $\mathrm{Sc}_t = \mathrm{Pr}_t$, $K_T = K_q$, and $\beta_{ap} = \beta$ as originally assumed in the 1926 manuscript of Bowen. To relax this assumption, a model is required to explain how K_T/K_q deviates from unity and is explored above water surfaces. Specifically, constraints on the magnitude of K_T/K_q and atmospheric stability regimes that elicit maximum deviations from unity are the sought-after outcomes. The trivial case when $R_{Tq} = \overline{T'q'}/(\sigma_T\sigma_q) = 1$ (perfect similarity) is not repeated here because it directly leads to $R_{wT} = R_{wq}$ and $K_T = K_q$ as discussed elsewhere [7]. For this reason, it is assumed through out that $|R_{Tq}| < 1$. It is noted that $|R_{Tq}| < 1$ places minor constraints on the magnitude of R_{wT}/R_{wq} as can be shown from the Gram determinant inequality [50] discussed elsewhere [39,51]. Hence, the product $|R_{Tq}R_{wT}/R_{wq}|$ can be unity or exceed unity even when $|R_{Tq}| < 1$.

B. Bringing the eddies into $\mathrm{Sc}_t/\mathrm{Pr}_t$

To arrive at expressions for $\mathrm{Sc}_t/\mathrm{Pr}_t$, contributions of various wave numbers k associated with the cospectra of turbulence are considered and are given as

$$\frac{K_T}{K_q} = \frac{\rho C_p}{L_v}\frac{\frac{d\overline{q}}{dz}}{\frac{d\overline{T}}{dz}}\frac{\int_0^\infty F_{wT}(k)dk}{\int_0^\infty F_{wq}(k)dk}, \tag{11}$$

where $F_{wT}(k)$ and $F_{wq}(k)$ are the cospectra for heat and water vapor fluxes, respectively, and k is interpreted as the 1-D wave number along $\overline{U}$. It can be shown that for stationary and planar homogeneous high Reynolds number flow in the absence of subsidence, these cospectra at any k can be approximated by [52–57]

$$F_{wT}(k) = \frac{-(1-C_I)\frac{d\overline{T}}{dz}F_{ww}(k) + (1-2\alpha_I)\beta_o F_{TT}(k)}{\left(1+\mathrm{Pr}_m^{-1}\right)\nu k^2 + A_R\tau(k)^{-1}}, \tag{12}$$

and

$$F_{wq}(k) = \frac{-(1-C_I)\frac{d\overline{q}}{dz}F_{ww}(k) + (1-2\alpha_I)\beta_o F_{Tq}(k)}{\left(1+\mathrm{Sc}_m^{-1}\right)\nu k^2 + A_R\tau(k)^{-1}}, \tag{13}$$

where A_R, C_I, and α_I are constants related to the Rotta closure model. Specifically, C_I is related to the isotropization of the production term and a value $C_I = 3/5$ has been predicted from rapid distortion theory [58]. An $\alpha_I = 1/3$ is predicted for isotropic turbulence [59] though the effects of ς on its magnitude remain uncertain, and $A_R = 1.8$ is the Rotta constant associated with the term describing the slow part of the pressure-scalar interaction as discussed elsewhere [60,61]. The $\tau(k) = \epsilon^{-1/3}k^{-2/3}$ is a wave-number-dependent relaxation time scale [62–65] that varies with the mean dissipation rate of TKE, ϵ, $F_{ww}(k)$ and $F_{TT}(k)$ are the vertical velocity and air temperature spectra, respectively, satisfying the normalizing properties $\int_0^\infty F_{ww}(k)dk = \sigma_{ww}^2$ and $\int_0^\infty F_{TT}(k)dk = \sigma_{TT}^2$, and $F_{Tq}(k)$ is the temperature-humidity cospectrum satisfying the normalizing property $\int_0^\infty F_{Tq}(k)dk = \overline{T'q'}$, and $\mathrm{Pr}_m \approx 0.7$ and $\mathrm{Sc}_m \approx 0.6$ are the molecular Prandtl and Schmidt numbers in air at standard temperature and pressure. Defining the Kolmogorov microscale as $\eta_{ko} = (\nu^3/\epsilon)^{1/4}$ [58,66], it directly follows that $(A_R\epsilon^{1/3}k^{2/3}) \gg [(1+\mathrm{Pr}_m^{-1})\nu k^2]$ when $k\eta_{ko} \ll [A_R/(1+\mathrm{Pr}_m^{-1})]^{3/4} \approx 0.7$. This condition implies that the molecular terms are only comparable to the pressure-scalar interaction term when $k\eta_{ko}$ is of order unity. Such small scales do not contribute appreciably to turbulent scalar or momentum fluxes and are ignored thereafter [58] due the high Re_* characterizing ASL flows (i.e., $\eta_{ko}/z \ll 1$). In terms of arbitrary spectral shapes, the wave-number integrated budget equation models are given by

$$\overline{w'T'} = \frac{1-C_I}{A_R}\frac{d\overline{T}}{dz}I_1\left[-1 + \frac{(1-2\alpha_I)\beta_o I_2}{(1-C_I)\frac{d\overline{T}}{dz}I_1}\right] \tag{14}$$

and

$$\overline{w'q'} = \frac{1-C_I}{A_R}\frac{d\overline{q}}{dz}I_1\left[-1 + \frac{(1-2\alpha_I)\beta_o I_3}{(1-C_I)\frac{d\overline{q}}{dz}I_1}\right], \tag{15}$$

where the integrals are given as

$$I_1 = \int_0^\infty \tau(k)F_{ww}(k)dk, \tag{16}$$

$$I_2 = \int_0^\infty \tau(k)F_{TT}(k)dk,$$

$$I_3 = \int_0^\infty \tau(k)F_{Tq}(k)dk. \tag{17}$$

The cospectrum can be linked to $F_{TT}(k)$ and the water vapor concentration spectrum $F_{qq}(k)$ using $F_{Tq}(k) = \mathrm{Coh}(T,q)[F_{TT}(k)F_{qq}(k)]^{1/2}$, where $\mathrm{Coh}(k)$ is the coherence spectrum. Regardless of the

spectral and cospectral shapes, these definitions yield

$$\frac{K_T}{K_q} = \frac{\left[-1 + \frac{(1-2\alpha_I)\beta_o I_2}{(1-C_I)\frac{d\overline{T}}{dz} I_1}\right]}{\left[-1 + \frac{(1-2\alpha_I)\beta_o I_3}{(1-C_I)\frac{d\overline{q}}{dz} I_1}\right]}. \tag{18}$$

As earlier mentioned, the numerical value for α_I appears uncertain in stratified high-Reynolds-number flows with $\alpha_I = 0$ suggested for stable flows [55] and $\alpha_I = 1/2$ estimated from large eddy simulation (LES) studies of the convective boundary layers [59,67]. If α_I increases from its isotropic value of $1/3$ to $1/2$, then $K_T/K_q = 1$ irrespective of any dissimilarity between heat and water vapor transport or stability regime.

C. Linking spectral shapes to K_T/K_q

Three cases are now considered with regards to the shapes of $\tau(k)$, $F_{ww}(k)$, $F_{TT}(k)$, and $F_{Tq}(k)$ that impact I_1, I_2, and I_3. These three cases are ordered from simple to complex, with the case 1 lumping all the effects of turbulence into a master time scale as common to higher-order Reynolds-averaged Navier-Stokes (RANS) closure models. The most complex case, case 3, accounts for all turbulent scales using realistic energy spectra derived from field measurements over lakes. Case 2 is intermediate and assumes all turbulent spectra follow Kolmogorov scaling [68] for all $1/h_o < k < \infty$, where h_o may be interpreted as the largest turbulent scale in the flow.

Case 1: The constant τ. In this case, $\tau(k)$ is replaced by a single effective relaxation time scale τ_{eff} acting equally on all k. This case highlights many common features between this approach and higher-order closure models that assign a single length or time scale to all turbulent eddies. With $\tau(k) = \tau_{\text{eff}}$ being independent of k, and when integrating across all k leads to $I_1 = \tau_{\text{eff}}\sigma_w^2$, $I_2 = \tau_{\text{eff}}\sigma_T^2$, and $I_3 = \tau_{\text{eff}}\overline{T'q'}$. Expressed in terms of stability correction functions, this modeled K_T/K_q reduces to

$$\frac{K_T}{K_q} = \frac{1 - \frac{1-2\alpha_I}{1-C_I}\frac{\varsigma}{\phi_h(\varsigma)}\left(\frac{\phi_{TT}(\varsigma)}{\phi_{ww}(\varsigma)}\right)^2}{1 - \frac{1-2\alpha_I}{1-C_I}R_{Tq}\frac{\varsigma}{\phi_v(\varsigma)}\left[\frac{\phi_{qq}(\varsigma)\phi_{TT}(\varsigma)}{(\phi_{ww}(\varsigma))^2}\right]}. \tag{19}$$

The similarity theory results for $\phi_v(\varsigma)$ and $\phi_{qq}(\varsigma)$ in the above expression are linked to their temperature counterparts $\phi_h(\varsigma)$ and $\phi_{TT}(\varsigma)$ through R_{Tq} and R_{wT}/R_{wq} to yield

$$\frac{K_T}{K_q} = \frac{1 - \frac{1-2\alpha_I}{1-C_I}\frac{\varsigma}{\phi_h(\varsigma)}\left(\frac{\phi_{TT}(\varsigma)}{\phi_{ww}(\varsigma)}\right)^2}{1 - R_{Tq}\left(\frac{K_T}{K_q}\right)^{-1}\left(\frac{R_{wT}}{R_{wq}}\right)\frac{1-2\alpha_I}{1-C_I}\frac{\varsigma}{\phi_h(\varsigma)}\left(\frac{\phi_{TT}(\varsigma)}{\phi_{ww}(\varsigma)}\right)^2}. \tag{20}$$

This solution can be recast as

$$\frac{K_T}{K_q} = \frac{1 - \Gamma_1(\varsigma)}{1 - \left(\frac{K_T}{K_q}\right)^{-1}\left(\frac{R_{wT}}{R_{wq}}\right)R_{Tq}\Gamma_1(\varsigma)}, \tag{21}$$

where the function

$$\Gamma_1(\varsigma) = \frac{1-2\alpha_I}{1-C_I}\frac{\varsigma}{\phi_h(\varsigma)}\left(\frac{\phi_{TT}(\varsigma)}{\phi_{ww}(\varsigma)}\right)^2. \tag{22}$$

Solving this expression for K_T/K_q yields

$$\frac{K_T}{K_q} = \frac{\text{Sc}_t}{\text{Pr}_t} = 1 + \Gamma_1(\varsigma)\left[\left(\frac{R_{wT}}{R_{wq}}\right)R_{Tq} - 1\right]. \tag{23}$$

This expression is identical to earlier ones derived from standard higher-order closure models [19,21] when the $(1-2\alpha_I)(1-C_I)^{-1}$ multiplier in Γ_1 is replaced by $1/2$. The $(1-2\alpha_I)(1-C_I)^{-1}$ multiplier originates from the isotropization of the production term here. The $\Gamma_1(\varsigma)$ is purposely

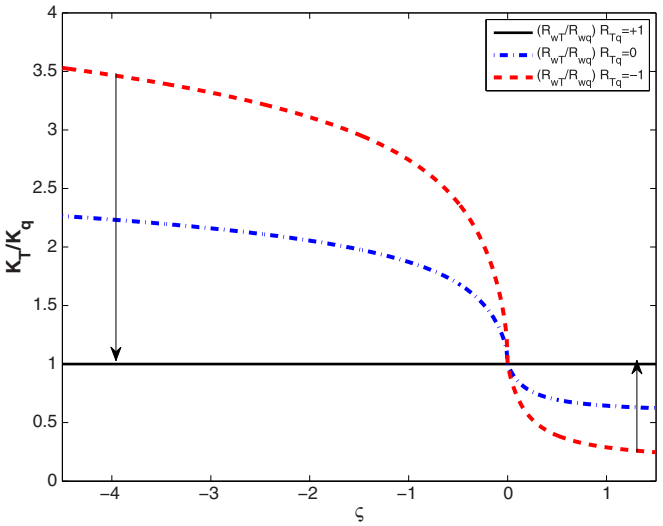

FIG. 1. Predicted variations of K_T/K_q with ς for case 1 using Eq. (23) for $(R_{wT}/R_{wq})R_{Tq} = +1$, $|(R_{wT}/R_{wq})R_{Tq}| = 0$, and $(R_{wT}/R_{wq})R_{Tq} = -1$ with $\alpha_I = 1/3$. Unstable and stable atmospheric stability conditions are delineated by $\varsigma < 0$ or $\varsigma > 0$, respectively. Arrows indicate increasing $(R_{wT}/R_{wq})R_{Tq}$ from -1 to $+1$.

formulated to be independent of water vapor statistics and all the water vapor effects on K_T/K_q are included in $(R_{wT}/R_{wq})R_{Tq}$. The function satisfies the condition $\Gamma_1(0) = 0$. The model here predicts a $K_T/K_q = 1$ when (1) $|\varsigma| \to 0$ (i.e., near-neutral conditions) or when (2) $(R_{wT}/R_{wq})R_{Tq} = 1$ (perfect similarity between heat and water vapor transport as discussed elsewhere [7]). While the expression here is only sensitive to the product $(R_{wT}/R_{wq})R_{Tq}$, the trivial case where $R_{Tq} = 1$ resulting in $R_{wT}/R_{wq} = 1$ recovers $K_T/K_q = 1$ irrespective of I_1, I_2, and I_3. The expression also delineates two other dynamically interesting regimes. The first is when $|(R_{wT}/R_{wq})R_{Tq}| = 0$ and the second regime is when $(R_{wT}/R_{wq})R_{Tq} = -1$. To illustrate the possible range of variability in K_T/K_q in these two regimes, standard ASL values for ϕ_{ww}, ϕ_{TT}, and ϕ_h are used in Fig. 1 predicting K_T/K_q.

For unstable conditions, $\varsigma < 0$:

$$\phi_{ww}(\varsigma) = A_{ww}\,(1 - 3\varsigma)^{\frac{1}{3}}; \quad \phi_{TT}(\varsigma) = 0.95(\varsigma)^{-1/3}; \tag{24}$$

$$\phi_h(\varsigma) = (1 - 16\varsigma)^{-1/2}. \tag{25}$$

For stable conditions, $\varsigma > 0$:

$$\phi_{ww}(\varsigma) = A_{ww} = 1.25\,; \quad \phi_{TT}(\varsigma) = A_{TT} = 2; \tag{26}$$

$$\phi_h(\varsigma) = 1 + b\varsigma; \quad b = 5. \tag{27}$$

It is evident that $K_T/K_q \geqslant 1$ are predicted for unstable conditions and $K_T/K_q \leqslant 1$ for stable conditions when $R_{wT}/R_{wq}R_{Tq} \neq 1$.

With this background and noting the association between K_T/K_q and $(R_{wT}/R_{wq})R_{Tq}$, it is instructive to ask how $(R_{wT}/R_{wq})R_{Tq}$ varies with atmospheric stability above water surfaces when $|R_{Tq}| < 1$. Figure 2 presents these variations using published data above two large lakes characterized by different climatic regimes and marine boundary layers. It is clear that much of the variations occur in near-neutral conditions where Eq. (23) predicts $K_T \approx K_q$ no matter what values $(R_{wT}/R_{wq})R_{Tq}$

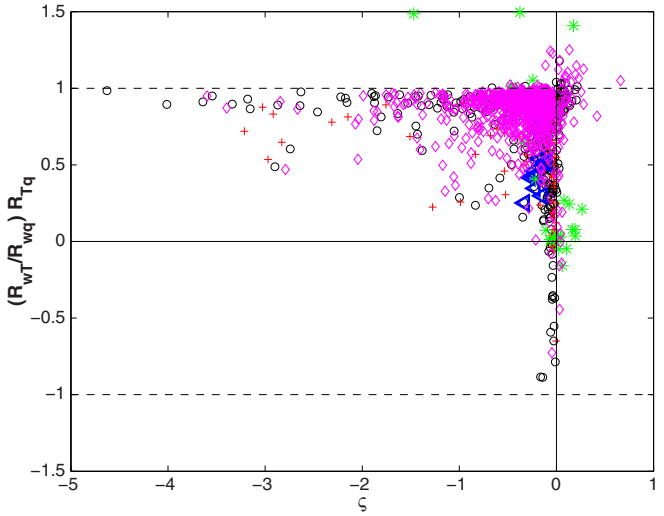

FIG. 2. Variation of measured $(R_{wT}/R_{wq})R_{Tq}$ with measured atmospheric stability parameter ς above Lake Leman, Switzerland (open circles), and Lake Kinneret, Israel (pluses), both described elsewhere [39], a marine boundary layer (stars) where heat and water vapor fluxes did not vary by more than 20% with height from the Riso Air-Sea Experiment (RASEX) described elsewhere [41], and a large inland water body in Mississippi (Ross Barnett Reservoir), USA (diamond), described elsewhere [69,70]. For reference, the 1969 San Diego and Barbados ocean experiments (triangles) are also shown (taken from Table 1 from Phelps and Pond [40]).

takes on. For unstable conditions, $(R_{wT}/R_{wq})R_{Tq}$ tends to be between 0.5 and 1.0, suggesting a $K_T/K_q \geqslant 1$. Again, few instances are noted when $-1 < (R_{wT}/R_{wq})R_{Tq} < 0$, but those instances appear to be rare and still associated with near-neutral conditions when Eq. (23) predicts $K_T \approx K_q$ due to $\Gamma_1(0) \approx 0$. For mildly stable conditions, $(R_{wT}/R_{wq})R_{Tq} \approx +1$, again suggesting that $K_T \approx K_q$. When interpreting Eq. (23) in this context, the data featured here suggest that much uncertainty in K_T/K_q appears to be associated with mildly unstable or mildly stable regimes, where $(R_{wT}/R_{wq})R_{Tq}$ varies appreciably and $\Gamma_1(\varsigma)$ remains finite.

Case 2: Inertial spectra. While imposing a single effective relaxation time recovers predictions from earlier closure models [19,21,22], it is unrealistic. To illustrate, consider the case when the spectra of turbulence are assumed to be inertial [71] and follow Kolmogorov [68] scaling from $k = 1/h_o$ to $k \to \infty$, where h_o is the largest scale of turbulence. For these idealized shapes (and for $\mathrm{Sc}_m \approx \mathrm{Pr}_m \approx 1$), the spectra $F_{ww}(k) = C_{ow}\epsilon^{2/3}k^{-5/3}$, $F_{TT}(k) = C_T\epsilon^{-1/3}N_Tk^{-5/3}$, $\epsilon = -\overline{u'w'}(d\overline{U}/dz) + \beta_o\overline{w'T'}$ are derived from a TKE budget that is in equilibrium [72,73], $N_T \approx -\overline{w'T'}(d\overline{T}/dz)$ is the half-variance temperature dissipation rate, $C_{ow} \approx 0.65$ is the Kolmogorov constant for the vertical velocity component [74], and $C_T \approx 0.8$ is the Kolmogorov-Obukhov-Corrsin constant for the temperature spectrum [36,75–77]. For these assumed spectra, $F_{wT} \sim k^{-7/3}$ expected in boundary layers [58,78–80]. If $\tau(k) = \tau_{\mathrm{eff}}$ as previously considered, then $F_{wT} \sim k^{-5/3}$, an unconventional cospectral scaling for the inertial subrange. For the second case then, the $\tau(k) = k^{-2/3}\epsilon^{-1/3}$ is considered instead of τ_{eff}. For reference, the vertical velocity, air temperature, and water vapor concentration spectra are all assumed to follow inertial subrange scaling laws unaffected by intermittency, large-scale or boundary effects, viscous cutoff, or bottlenecks [81]. For these idealized spectral shapes, and upon integration across all scales bounded by $1/h_o \leqslant k \leqslant \infty$ yields for I_1 and I_2 the following:

$$I_1 = \tfrac{3}{4}C_{ow}\epsilon^{1/3}h_o^{4/3}, \quad I_2 = \tfrac{3}{4}C_T\epsilon^{-2/3}N_Th_o^{4/3}. \tag{28}$$

To evaluate I_3, assumptions about the shape of $F_{Tq}(k)$ and $F_{qq}(k)$ are required. Here, $F_{qq}(k) = C_q\epsilon^{-1/3}N_qk^{-5/3}$, $C_q \approx C_T$ [36] is the Kolmogorov constant for the water vapor concentration

spectrum in the inertial subrange and N_q is the half-variance dissipation rate of q'. A model of maximum simplicity is to set the coherence spectrum a constant $A_{T,q}$ but constrained by the condition $|A_{T,q}| < 1$ to ensure $|R_{Tq}| < 1$ at all $1/h_o < k < \infty$ so that

$$F_{Tq}(k) = A_{T,q}(C_T C_q)^{1/2}\epsilon^{-1/3}(N_T N_q)^{1/2}k^{-5/3}, \tag{29}$$

where $A_{T,q}$ is determined from the normalizing property $\int_{1/h_o}^{\infty} F_{tq}(k)dk = \overline{T'q'}$ to yield

$$A_{T,q} = \frac{2}{3}\frac{\overline{T'q'}}{(C_T C_q)^{1/2}\epsilon^{-1/3}(N_T N_q)^{1/2}h_o^{2/3}}. \tag{30}$$

With this $A_{T,q}$ estimate, $F_{Tq}(k) = (2/3)\overline{T'q'}h_o^{-2/3}k^{-5/3}$ and I_3 is now given by

$$I_3 = \tfrac{1}{2}\overline{T'q'}\epsilon^{-1/3}h_o^{2/3}. \tag{31}$$

There is some support for a near-constant Coh(k) shape over land and water [40,82] when $kz < 1$. As expected, this assumption fails when $kz \gg 1$ as Coh(T,q) $\to 0$ due to the isotropic nature of small-scale eddies. These estimates of I_1, I_2, and I_3 result in

$$\frac{K_T}{K_q} = \frac{1 + \Gamma_2(\varsigma)}{1 + \left(\frac{K_T}{K_q}\right)^{-1} R_{Tq}\frac{R_{wT}}{R_{wq}}\Gamma_2(\varsigma)\theta_2(\varsigma)}, \tag{32}$$

where

$$\Gamma_2(\varsigma) = \frac{1 - 2\alpha_I}{1 - C_I}\frac{C_T}{C_{ow}}\frac{\varsigma}{\phi_m(\varsigma) - \varsigma}, \tag{33}$$

$$\theta_2(\varsigma) = \frac{2}{3}\frac{1}{C_T}\frac{(\phi_m(\varsigma) - \varsigma)^{1/3}(\phi_{TT}(\varsigma))^2}{\phi_h(\varsigma)}\left(\frac{\kappa z}{h_o}\right)^{2/3}. \tag{34}$$

Solving for K_T/K_q leads to

$$\frac{K_T}{K_q} = 1 + \Gamma_2(\varsigma)\left[R_{Tq}\frac{R_{wT}}{R_{wq}}\theta_2(\varsigma) - 1\right]. \tag{35}$$

As before, $\Gamma_2(0) = 0$ and corrections to K_T/K_q are only significant when $|\varsigma| > 0$ (i.e., thermally stratified flow). However, this solution differs from earlier outcomes in several ways: (1) it shows that K_T/K_q is influenced by $\phi_m(\varsigma)$ whereas the previous solutions were influenced by $\phi_{ww}(\varsigma)$, (2) the multiplier θ_2 is not unity and itself varies with atmospheric stability conditions whereas previous solutions suggest $\theta_2 = 1$, and (3) z/h_o emerges as a significant quantity that need not be a constant when h_o scales with the ABL height (instead of z as in previous solutions). For example, when $z/h_o \ll 1$, $\theta_2 \approx 0$, and K_T/K_q becomes decoupled from any dissimilarity in scalar transport characterized by $R_{Tq}(R_{wT}/R_{wq})$ but still varies with ς. This result, which only applies for $|R_{Tq}| < 1$, could not have been foreshadowed by earlier models.

Case 3: Realistic spectra. The third case considers realistic spectral shapes in the ASL for $F_{ww}(k)$, $F_{TT}(k)$, and $F_{qq}(k)$ instead of inertial subrange scaling, again assuming $|R_{Tq}| < 1$. The spectral shapes to be specified are approximations to measurements reported in Fig. 3. For analytical tractability, only the essential features of these measured spectra in Fig. 3 are described: A wave number $k_a = 1/z$ delineates large scales from inertial scale eddies in w' so that $F_{ww}(k) = C_{ow}\epsilon^{2/3}k_a^{-5/3}$ represents the spectrum for $kz < 1$ (i.e., a flat spectrum) and $F_{ww}(k) = C_{ow}\epsilon^{2/3}k^{-5/3}$ describes the spectrum for $kz > 1$, an oversimplification here. Likewise, $\tau(k) = \epsilon^{-1/3}k_a^{-2/3}$ for $kz < 1$ and $\tau(k) = \epsilon^{-1/3}k^{-2/3}$ for $kz > 1$. With regards to $F_{TT}(k)$, three regimes are identified: The inertial regime with $F_{TT}(k) = C_T\epsilon^{-1/3}N_T k^{-5/3}$ for $kz > 1$ as with $F_{ww}(k)$, the production regime given as $F_{TT}(k) = C_p T_*^2 k^{-1}$ for $h_o^{-1} < k < z^{-1}$, where upon matching this regime to the inertial at $k_a z = 1$ yields an estimate for the constant $C_p = C_T\kappa^{-2/3}\phi_h(\varsigma)(\phi_m(\varsigma) - \varsigma)^{-1/3}$. While the data in Fig. 3 cannot resolve many aspects of the regime associated with very large scales

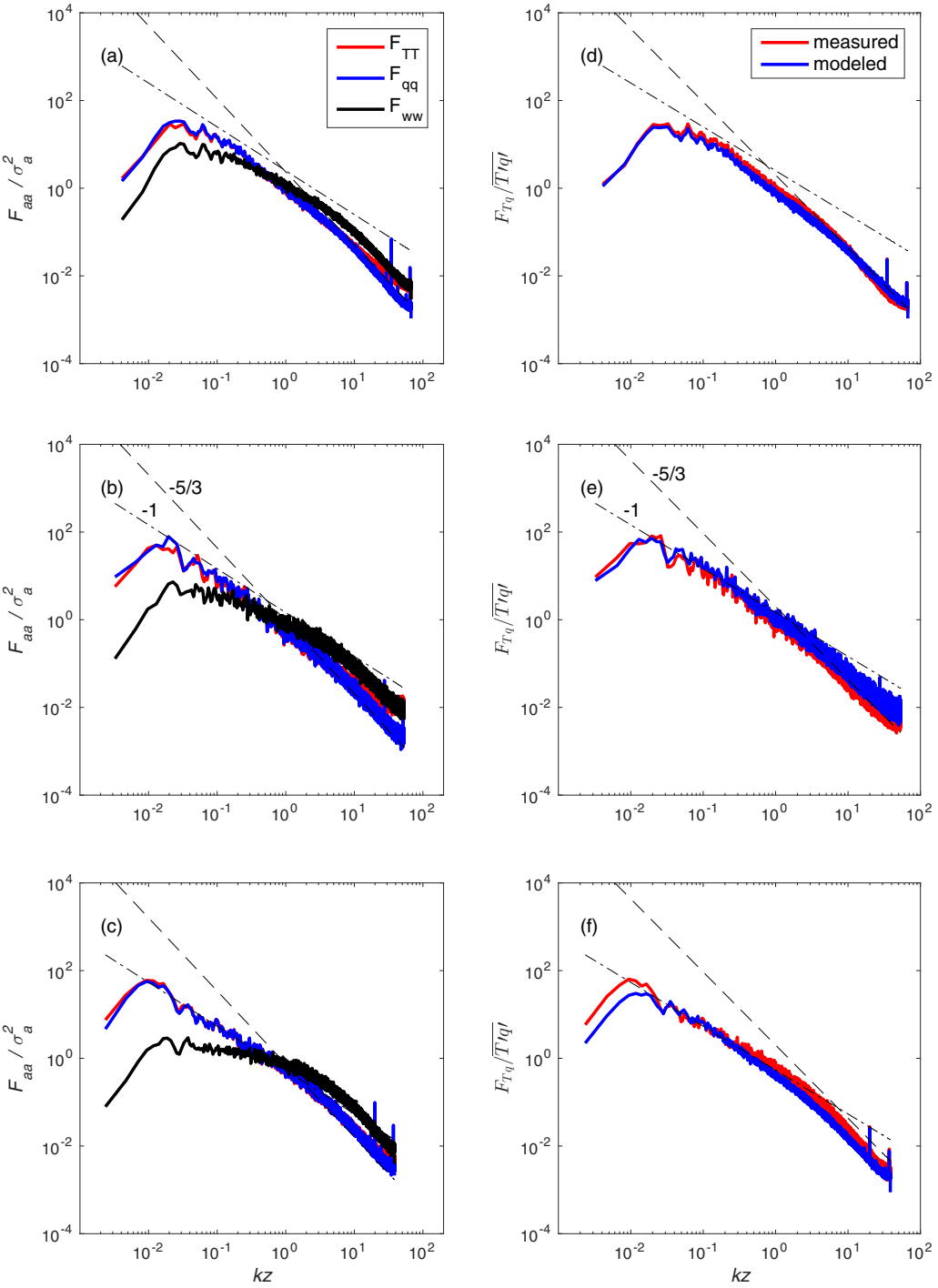

FIG. 3. Left: Variations of ensemble measured $F_{ww}(k)/\sigma_w^2$ ($a = w'$), $F_{TT}(k)/\sigma_T^2$ ($a = T'$), $F_{qq}(k)/\sigma_q^2$ ($a = q'$) with normalized wave number kz for conditions $R_{Tq} > 0.5$ (top), $-0.5 < R_{Tq} < 0.5$ (middle), and $R_{Tq} < -0.5$ (bottom) collected above Lake Leman, Switzerland. For reference, the -1 and $-5/3$ power laws are shown. Right: Comparison between measured and modeled $F_{Tq}(k)$ ($a = T', b = q'$) using measured $F_{TT}(k)/\sigma_T^2$ and $F_{qq}(k)/\sigma_q^2$ but setting A_{Tq} (the coherence spectrum) to a constant independent of k.

($kh_o < 1$), the model calculations next are based on $F_{TT}(k) = C_p T_*^2 (z/h_o)^{-1}$ being a constant for such scales extending to $k = 0$. The shape of $F_{qq}(k)$ is assumed to be similar to $F_{TT}(k)$, which is also supported by the measurements in Fig. 3. The conditions promoting the onset of a -1 power law in $F_{TT}(k)$ for $|\varsigma| < 1$ are reviewed elsewhere [83] and are not repeated here. The scale h_o is also unambiguously interpreted as a length scale that varies in proportion to the boundary layer height.

Carrying out the integration for each region, the resulting I_1 is

$$I_1 = \tfrac{7}{4} C_{ow} \epsilon^{1/3} z^{4/3}, \tag{36}$$

and

$$I_2 = \left[\frac{7}{4} + \ln\left(\frac{h_o}{z}\right)\right] C_T N_T \epsilon^{-2/3} z^{4/3}. \tag{37}$$

Again, for the purposes of determining I_3, it is assumed that $F_{Tq}(k) = A_{Tq}\sqrt{F_{TT}(k)F_{qq}(k)}$ with $|A_{Tq}| < 1$ being constant across scales and can be evaluated from the normalizing property as

$$A_{Tq} = \frac{\overline{T'q'}}{\left[\frac{5}{2} + \ln\left(\frac{h_o}{z}\right)\right]\sqrt{C_T C_q}\sqrt{N_T N_q}\,\epsilon^{-1/3} z^{2/3}}. \tag{38}$$

With this estimate for A_{Tq},

$$I_3 = \frac{\left[\frac{7}{4} + \ln\left(\frac{h_o}{z}\right)\right]}{\left[\frac{5}{2} + \ln\left(\frac{h_o}{z}\right)\right]} \overline{T'q'} \epsilon^{-1/3} z^{2/3}. \tag{39}$$

Support for such approximation to $F_{Tq}(k)$ with A_{Tq} being held constant across scales is also shown in Fig. 3. Acceptable agreement between model calculations driven by measured $F_{TT}(k)$ and $F_{qq}(k)$ and measured $F_{Tq}(k)$ is noted across all k.

Solving for K_T/K_q leads to

$$\frac{K_T}{K_q} = 1 + \Gamma_3(\varsigma)\left[R_{Tq}\frac{R_{wT}}{R_{wq}}\theta_3(\varsigma) - 1\right], \tag{40}$$

where

$$\Gamma_3(\varsigma) = \left[1 + \frac{4}{7}\ln\left(\frac{h_o}{z}\right)\right]\frac{1 - 2\alpha_I}{1 - C_I}\frac{C_T}{C_{ow}}\frac{\varsigma}{\phi_m(\varsigma) - \varsigma}, \tag{41}$$

$$\theta_3(\varsigma) = \frac{1}{\left[\frac{5}{2} + \ln\left(\frac{h_o}{z}\right)\right]}\frac{(\kappa)^{2/3}}{C_T}\frac{[\phi_m(\varsigma) - \varsigma]^{1/3}[\phi_{TT}(\varsigma)]^2}{\phi_h(\varsigma)}. \tag{42}$$

As before, $\Gamma_3(0) = 0$ ensures that $K_T/K_q = 1$ for near-neutral conditions. However, dissimilarity in the shapes of $F_{ww}(k)$ and $F_{TT}(k)$ now results in $\ln(h_o/z)$ impacting both Γ_3 and θ_3 instead of θ_2 only (as for the inertial spectra case) but in opposite ways. For a given ς, increasing $\ln(h_o/z)$ increases $|\Gamma_3|$ and reduces θ_3. As before, reductions in θ_3 reduce sensitivity of K_T/K_q on $R_{Tq}R_{wT}/R_{wq}$. Amplifications in $|\Gamma_3|$ associated with increased h_o/z enhance the active role of temperature on K_T/K_q.

To explore the effects of z/h_o along with $(R_{wT}/R_{wq})R_{Tq}$, a comparison between models for cases 2 (inertial spectra) and 3 (realistic spectra) is featured in Fig. 4 for $\alpha_I = 1/3$ (i.e., isotropic limit). Typical daytime $z/h_o = 0.01$ (labeled hereafter as small z/h_o) as well as $z/h_o = 0.5$ (labeled hereafter as large z/h_o) expected in stable conditions when h_o collapses are used to illustrate h_o effects above and beyond ς. For case 2, increasing z/h_o from 0.01 to 0.5 increases θ_2 and $K_T/K_q(\neq 1)$ becomes sensitive to $(R_{wT}/R_{wq})R_{Tq}$. For the larger z/h_o in case 2, $K_T/K_q \leqslant 1$ for unstable conditions even when $(R_{wT}/R_{wq})R_{Tq} = 1$, which cannot be reproduced by case 1 (i.e., using a single τ_{eff}). As expected for case 1, $(R_{wT}/R_{wq})R_{Tq} = 1$ results in $K_T/K_q = 1$ for

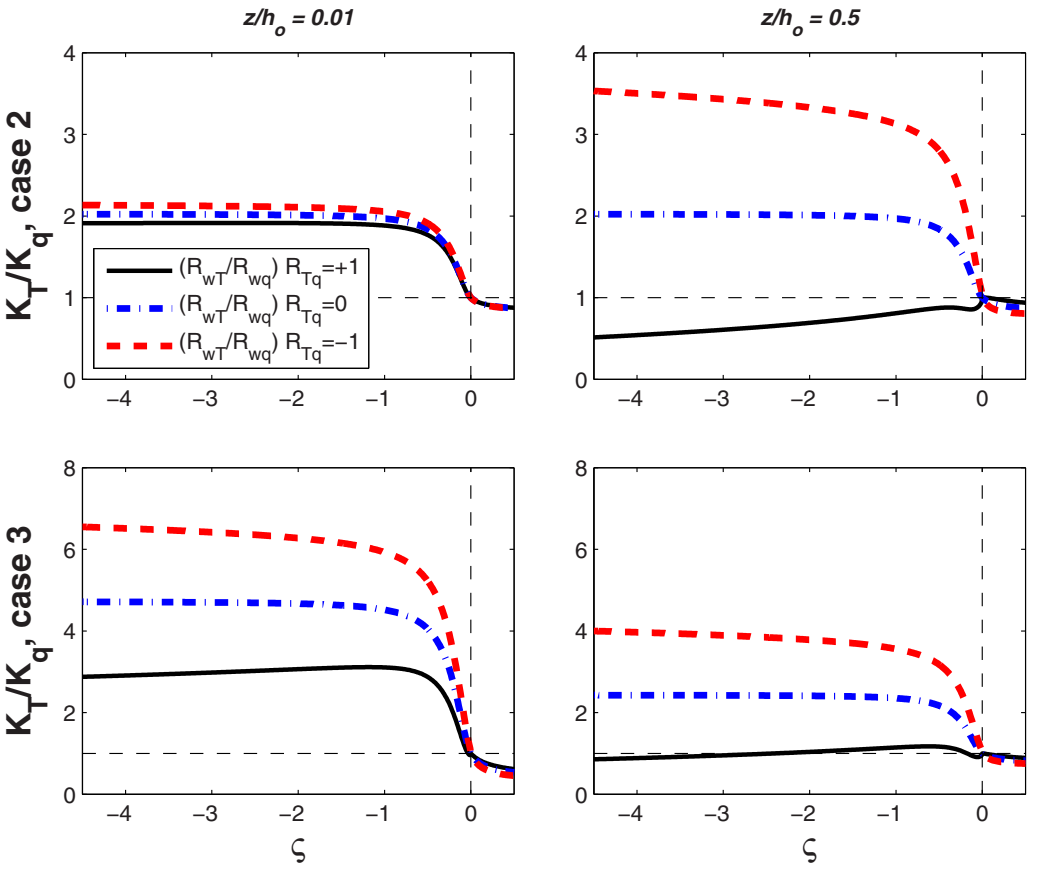

FIG. 4. Comparison between modeled K_T/K_q variations with ς for $z/h_o = 0.01$ (typical for unstable atmospheric states) and $z/h_o = 0.5$ (that can occur for stable atmospheric states) using $\alpha_I = 1/3$. The model runs assume $|R_{Tq}| < 1$ but $(R_{wT}/R_{wq})R_{Tq}$ can take on arbitrary values. The top panels are for case 2 (inertial spectra) and bottom panels are for case 3 (realistic spectra).

all stability regimes. For the smallest z/h_o, the expressions here suggest a decoupling between K_T/K_q and variations in $(R_{wT}/R_{wq})R_{Tq}$ for case 2 (where $\theta_2 \sim (z/h_o)^{2/3}$ becomes small) but not case 3 (where $\theta_3 \sim [(5/2) + \log(h_o/z)]^{-1}$ remains appreciable for typical z/h_o values). Maximum deviations from unity in K_T/K_q are associated with case 3 and largest h_o (or smallest z/h_o). For case 3, the dependency of K_T/K_q on $(R_{wT}/R_{wq})R_{Tq}$ is far significant when compared to the previous two cases where h_o is large (or z/h_o is small). For the largest z/h_o, $K_T/K_q \approx 1$ when $(R_{wT}/R_{wq})R_{Tq} \approx 1$ in case 3 as in case 1.

D. Comparison with experiments

The three expressions for K_T/K_q covered in cases 1 to 3 are now compared against independent estimates using data collected above a large inland water body (Ross Barnett Reservoir, Mississippi, USA) described elsewhere [69,70] in Fig. 5. The measurements include the following: $\overline{w'q'}$, $\overline{w'T'}$, $\overline{w'w'}$, $\overline{q'q'}$, $\overline{T'T'}$, $\overline{T'q'}$, $\overline{w'u'}$ at 10-Hz sampling frequency with averaging conducted over 30-min intervals, as well as $\overline{T_s}$, $\overline{T}$, and $\overline{q}$ at $z = 4$ m. The h_o was not measured in the experiment but was estimated using the expression $h_o = C_z u_*/f_{\rm cor}$, where $C_z = 0.3$ is a similarity constant inferred for near-neutral conditions, and $f_{\rm cor} = 1 \times 10^{-4}$ rad s^{-1} is the Coriolis frequency [84]. This estimate likely under-estimates h_o in convective conditions and overestimates h_o in stable

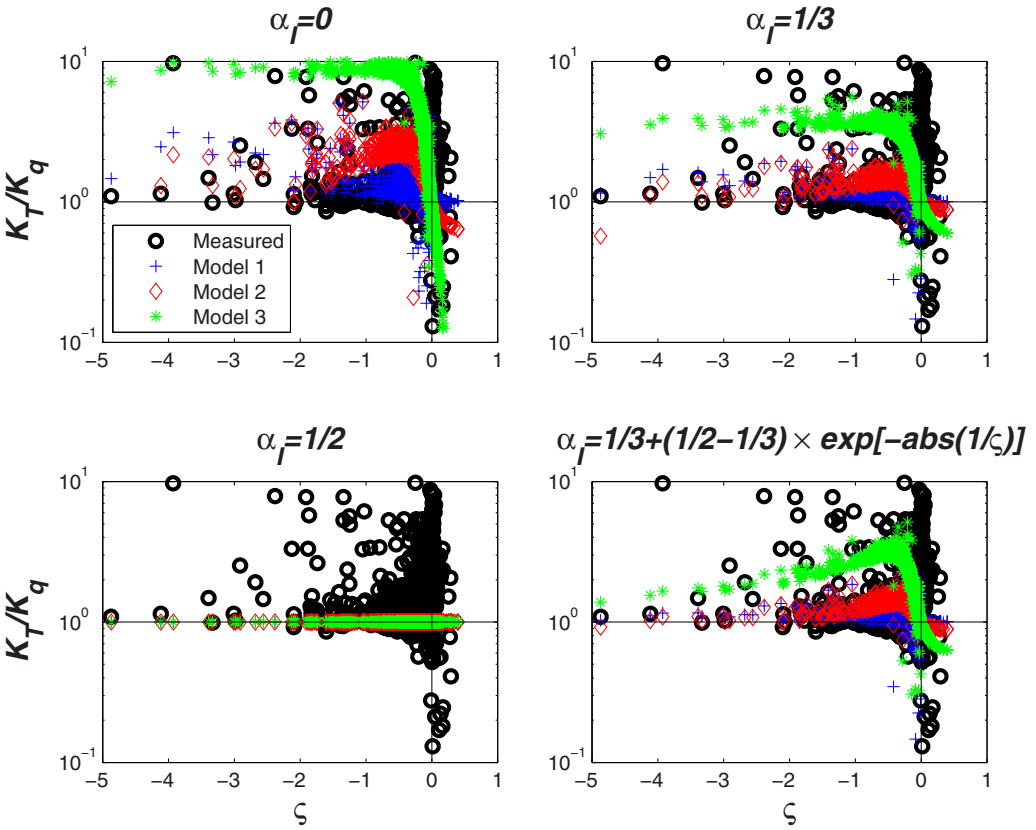

FIG. 5. Comparison between modeled K_T/K_q with ς using estimated h_o [84] and measured $(R_{wT}/R_{wq})R_{Tq}$ for the Ross Barnett Reservoir (Mississippi, USA) for various α_I to illustrate model sensitivity. Models 1, 2, and 3 correspond to the final formulation in cases 1, 2, and 3, respectively, but using measured $R_{Tq}R_{wT}/R_{wq}$ shown in Fig. 2.

conditions. Given the uncertainty in α_I, the comparison in Fig. 5 is conducted for $\alpha_I = 0$, $\alpha_I = 1/3$ (isotropic case), $\alpha_I = 1/2$ (suggested for convective conditions from LES studies), and an ad hoc stability dependent $\alpha_I = 1/3 + (1/2 - 1/3) \times \exp[-|\varsigma^{-1}|]$. This functional dependency ensures that $\alpha_I \approx 1/3$ for near-neutral conditions ($|\varsigma| \approx 0$) and $\alpha_I \approx 1/2$ for near-convective conditions ($-\varsigma \to \infty$). When $\alpha_I = 1/3$, cases 1 and 2 reasonably agree with the independent estimates in Fig. 5 that $K_T/K_q > 1$ for moderate to strongly unstable conditions. Case 3 captures the rapid rise in K_T/K_q as atmospheric stability regime transitions from its near-neutral to mildly unstable state (especially for $\alpha_I = 0$), but overestimates K_T/K_q. The overestimation is not surprising as the spectral shapes assumed for case 3 are appropriate for near-neutral and mildly unstable flow whereas air temperature and vertical spectra tend to follow an approximate $-5/3$ scaling for strongly unstable conditions (i.e., resembling the analysis in case 2). As expected, reducing α_I from its $1/2$ value increases modeled K_T/K_q, especially for the formulation in case 3. The stability-dependent α_I prescribed here results in a nonmonotonic shape for modeled K_T/K_q, especially for the formulations covered in cases 2 and 3. Hence, it is evident here that K_T/K_q variations are sensitive to deviations in α_I from $1/2$ though in the absence of any other guidance, setting $\alpha_I = 1/3$ appears plausible for cases 1 and 2 for unstable conditions, and case 3 for near-neutral to transitioning to unstable conditions.

III. CONCLUSION

The three expressions for K_T/K_q derived for the nontrivial case $|R_{Tq}| < 1$ but arbitrary $R_{Tq}R_{wT}/R_{wq}$ are the sought results. The $|R_{Tq}| < 1$ in the atmosphere is guaranteed by the near anticorrelation at the top of the atmospheric boundary layer. Attainment of $K_T/K_q \approx 1$ is due to a competition between the active role of temperature encoded here in Γ_1, Γ_2, and Γ_3 and dissimilarity in heat and water vapor transport as captured by the term $(R_{wT}/R_{wq})R_{Tq}$. A $K_T/K_q = 1$ emerges from all cases when (i) $|\varsigma| \to 0$ no matter what h_o/z or $(R_{wT}/R_{wq})R_{Tq}$ values they take. Also, $K_T/K_q = 1$ for any $|\varsigma|$, $z/h_o < 1$ or $(R_{wT}/R_{wq})R_{Tq}$ if α_I is increased to $1/2$ (suggested by some LES studies for convective boundary layers). In other cases, $K_T/K_q \neq 1$ even when $(R_{wT}/R_{wq})R_{Tq} = 1$ (provided $R_{Tq} < 1$) in cases 2 and 3, but not in case 1.

In summary, the work here (cases 2 and 3) demonstrated that when $|R_{Tq}| < 1$, deviations in K_T/K_q from unity depend on z/L and z/h_o as well as the dissimilarity measure $(R_{wT}/R_{wq})R_{Tq}$. The sensitivity of K_T/K_q to z/L, z/h_o and $(R_{wT}/R_{wq})R_{Tq}$ is also influenced by the spectral shapes of vertical velocity, air temperature, and water vapor. Such sensitivity cannot be inferred from classical higher-order closure schemes that utilize a master length or time scale.

ACKNOWLEDGMENTS

G.K. acknowledges support from the National Science Foundation (NSF-EAR-1344703), and the U.S. Department of Energy (DE-SC0006967 and DE-SC0011461). The Lake Leman data were collected by the Environmental Fluid Mechanics and Hydrology Laboratory of Professor M. Parlange at EPFL. We thank Professor Parlange for sharing the data with us.

---

[1] J Boussinesq, *Essai sur la théorie des eaux courantes* (Imprimerie Nationale, Paris, France, 1877).
[2] W. D. McComb, *Renormalization Methods: A Guide for Beginners* (Clarendon Press, Oxford, 2004).
[3] I. S. Bowen, The ratio of heat losses by conduction and by evaporation from any water surface, Phys. Rev. **27**, 779 (1926).
[4] J. M. Lewis, The story behind the Bowen ratio, Bull. Am. Meteorol. Soc. **76**, 2433 (1995).
[5] T. W. Yu, Parameterization of surface evaporation rate for use in numerical modeling, J. Appl. Meteorol. **16**, 393 (1977).
[6] G. L. Mellor and T. Yamada, Development of a turbulence closure model for geophysical fluid problems, Rev. Geophys. **20**, 851 (1982).
[7] R. J. Hill, Implications of Monin-Obukhov similarity theory for scalar quantities, J. Atmos. Sci. **46**, 2236 (1989).
[8] W. T. Liu, Moisture and latent heat flux variabilities in the tropical pacific derived from satellite data, J. Geophys. Res.: Oceans **93**, 6749 (1988).
[9] P. Thadathil, Y. Sugimori, and M. Akiyama, Surface heat fluxes using satellite observations: A case study in the northwest pacific, J. Atmos. Ocean. Technol. **12**, 1071 (1995).
[10] R. Crago and W. Brutsaert, Daytime evaporation and the self-preservation of the evaporative fraction and the bowen ratio, J. Hydrol. **178**, 241 (1996).
[11] Y. H. Jo, X. H. Yan, J. Pan, M. X. He, and W. T. Liu, Calculation of the Bowen ratio in the tropical Pacific using sea surface temperature data, J. Geophys. Res.: Oceans **107**, 3134 (2002).
[12] P. L. Nagler, R. L. Scott, C. Westenburg, J. R. Cleverly, E. P. Glenn, and A. R. Huete, Evapotranspiration on western US rivers estimated using the enhanced vegetation index from modis and data from eddy covariance and Bowen ratio flux towers, Remote Sens. Environ. **97**, 337 (2005).
[13] K. Wang, Z. Li, and M. Cribb, Estimation of evaporative fraction from a combination of day and night land surface temperatures and NDVI: A new method to determine the Priestley-Taylor parameter, Remote Sens. Environ. **102**, 293 (2006).

[14] J. R. Philip, A physical bound on the Bowen ratio, J. Clim. Appl. Meteorol. **26**, 1043 (1987).
[15] E. L. Andreas, Comments on physical bound on the Bowen ratio, J. Appl. Meteorol. **28**, 1252 (1989).
[16] E. L. Andreas and B. A. Cash, A new formulation for the Bowen ratio over saturated surfaces, J. Appl. Meteorol. **35**, 1279 (1996).
[17] E. L. Andreas, R. E. Jordan, L. Mahrt, and D. Vickers, Estimating the Bowen ratio over the open and ice-covered ocean, J. Geophys. Res.: Oceans **118**, 4334 (2013).
[18] X. Guo, H. Liu, and K. Yang, On the application of the Priestley-Taylor relation on sub-daily time scales, Boundary-Layer Meteorol. **156**, 489 (2015).
[19] Z. Warhaft, Heat and moisture flux in the stratified boundary layer, Quarterly J. Roy. Meteorol. Soc. **102**, 703 (1976).
[20] R. A. Brost, Some comments on the turbulent exchange coefficients for sensible heat and water vapor under advective conditions, J. Appl. Meteorol. **18**, 378 (1979).
[21] N. L. Dias and W. Brutsaert, Similarity of scalars under stable conditions, Boundary-Layer Meteorol. **80**, 355 (1996).
[22] G. G. Katul and C. I. Hsieh, A note on the flux-variance similarity relationships for heat and water vapour in the unstable atmospheric surface layer, Boundary-Layer Meteorol. **90**, 327 (1999).
[23] G. Katul, S. M. Goltz, C. I. Hsieh, Y. Cheng, F. Mowry, and J. Sigmon, Estimation of surface heat and momentum fluxes using the flux-variance method above uniform and non-uniform terrain, Boundary-Layer Meteorol. **74**, 237 (1995).
[24] H. A. R. De Bruin, B. J. J. M. Van Den Hurk, and L. J. M. Kroon, On the temperature-humidity correlation and similarity, Boundary-Layer Meteorol. **93**, 453 (1999).
[25] F. Pasquill, Eddy diffusion of water vapour and heat near the ground, Proc. R. Soc. London A **198**, 116 (1949).
[26] N. E. Rider, Eddy diffusion of momentum, water vapour, and heat near the ground, Philos. Trans. Royal Soc. London, Ser. A **246**, 481 (1954).
[27] S. B. Verma, N. J. Rosenberg, and B. L. Blad, Turbulent exchange coefficients for sensible heat and water vapor under advective conditions, J. Appl. Meteorol. **17**, 330 (1978).
[28] A. R. G. Lang, K. G. McNaughton, C. Fazu, E. F. Bradley, and E. Ohtaki, Inequality of eddy transfer coefficients for vertical transport of sensible and latent heats during advective inversions, Boundary-Layer Meteorol. **25**, 25 (1983).
[29] G. Papaioannou, C. Jacovides, and P. Kerkides, Atmospheric stability effects on eddy transfer coefficients and on Penman's evaporation estimates, Water Res. Man. **3**, 315 (1989).
[30] X. Lee, Q. Yu, X. Sun, J. Liu, Q. Min, Y. Liu, and X. Zhang, Micrometeorological fluxes under the influence of regional and local advection: A revisit. Agricult. Forest Meteorol. **122**, 111 (2004).
[31] J. Huang, X. Lee, and E. G. Patton, Dissimilarity of scalar transport in the convective boundary layer in inhomogeneous landscapes, Boundary-Layer Meteorol. **130**, 327 (2009).
[32] S. Irmak, A. Kilic, and S. Chatterjee, On the equality assumption of latent and sensible heat energy transfer coefficients of the bowen ratio theory for evapotranspiration estimations: Another look at the potential causes of inequalities, Climate **2**, 181 (2014).
[33] N. J. Bink, The ratio of eddy diffusivities for heat and water vapour under conditions of local advection, Phys. Chem. Earth **21**, 119 (1996).
[34] J. C. Kaimal, J. C. Wyngaard, Y. Izumi, and O. R. Coté, Spectral characteristics of surface-layer turbulence, Quart. J. Royal Meteorol. Soc. **98**, 563 (1972).
[35] W. H. Brutsaert, *Evaporation into the Atmosphere* (D. Reidel, Dordrecht, 1982).
[36] U. L. F. Högström, Review of some basic characteristics of the atmospheric surface layer, Boundary-Layer Meteorol. **78**, 215 (1996).
[37] D. Li, E. Bou-Zeid, and H. A. R. De Bruin, Monin-Oobukhov similarity functions for the structure parameters of temperature and humidity, Boundary-Layer Meteorol. **145**, 45 (2012).
[38] S. Assouline, S. W. Tyler, J. Tanny, S. Cohen, E. Bou-Zeid, M. B. Parlange, and G. G. Katul, Evaporation from three water bodies of different sizes and climates: Measurements and scaling analysis, Adv. Water Res. **31**, 160 (2008).

[39] S. Assouline, D. Li, S. Tyler, J. Tanny, S. Cohen, E. Bou-Zeid, M. Parlange, and G. G. Katul, On the variability of the Priestley-Taylor coefficient over water bodies, Water Resour. Res. **52**, 150 (2016).
[40] G. T. J. Phelps and S. Pond, Spectra of the temperature and humidity fluctuations and of the fluxes of moisture and sensible heat in the marine boundary layer, J. Atmos. Sci. **28**, 918 (1971).
[41] G. G. Katul, A. M. Sempreviva, and D. Cava, The temperature-humidity covariance in the marine surface layer: A one-dimensional analytical model, Boundary-Layer Meteorol. **126**, 263 (2008).
[42] D. M. Cancelli, M. Chamecki, and N. L. Dias, A large-eddy simulation study of scalar dissimilarity in the convective atmospheric boundary layer, J. Atmos. Sci. **71**, 3 (2014).
[43] J. Laubach, K. G. McNaughton, and J. D. Wilson, Heat and water vapour diffusivities near the base of a disturbed stable internal boundary layer, Boundary-Layer Meteorol. **94**, 23 (2000).
[44] S. B. Pope, A more general effective-viscosity hypothesis, J. Fluid Mech. **72**, 331 (1975).
[45] S. E. Belcher and J. C. R. Hunt, Turbulent flow over hills and waves, Annu. Rev. Fluid Mech. **30**, 507 (1998).
[46] A. S. Monin and A. M. Obukhov, Basic laws of turbulent mixing in the surface layer of the atmosphere, Contrib. Geophys. Inst. Acad. Sci. USSR **24**, 163 (1954).
[47] A. S. Monin and A. M. Yaglom, *Statistical Fluid Mechanics*, Vol. 1 (MIT Press, Cambridge, MA, 1971), p. 873.
[48] A. M. Obukhov, Turbulence in an Atmosphere with a Non-uniform Temperature, Trudy Inst. Theor. Geofiz. Akad. Nauk SSSR **1**, 95 (1946).
[49] G. A. McBean and M. Miyake, Turbulent transfer mechanisms in the atmospheric surface layer, Quart. J. Royal Meteorol. Soc. **98**, 383 (1972).
[50] R. Courant and D. Hilbert, *Methods of Mathematical Physics*, Vol. 1 (John Wiley and Sons, New York, 1953).
[51] N. J. Bink and A. G. C. A. Meesters, Comment on Estimation of surface heat and momentum fluxes using the flux-variance method above uniform and non-uniform terrain by Katul et al. (1995), Boundary-Layer Meteorol. **84**, 497 (1997).
[52] S. Panchev, *Random Functions and Turbulence* (Pergamon Press, Oxford, 1971).
[53] G. G. Katul, A. Porporato, C. Manes, and C. Meneveau, Co-spectrum and mean velocity in turbulent boundary layers, Phys. Fluids **25**, 091702 (2013).
[54] G. G. Katul, D. Li, M. Chamecki, and E. Bou-Zeid, Mean scalar concentration profile in a sheared and thermally stratified atmospheric surface layer, Phys. Rev. E **87**, 023004 (2013).
[55] G. G. Katul, A. Porporato, S. Shah, and E. Bou-Zeid, Two phenomenological constants explain similarity laws in stably stratified turbulence, Phys. Rev. E **89**, 023007 (2014).
[56] D. Li, G. G. Katul, and E. Bou-Zeid, Turbulent energy spectra and cospectra of momentum and heat fluxes in the stable atmospheric surface layer, Boundary-Layer Meteorol. **157**, 1 (2015).
[57] D. Li, G. G. Katul, and S. Zilitinkevich, Revisiting the turbulent Prandtl number in an idealized atmospheric surface layer, J. Atmos. Sci. **72**, 2394 (2015).
[58] S. B. Pope, *Turbulent Flows* (Cambridge University Press, Cambridge, MA, 2000).
[59] C. H. Moeng and J. C. Wyngaard, An analysis of closures for pressure-scalar covariances in the convective boundary layer, J. Atmos. Sci. **43**, 2499 (1986).
[60] B. Launder, G. Reece, and W. Rodi, Progress in the development of a Reynolds-stress turbulence closure, J. Fluid Mech. **68**, 537 (1975).
[61] K. A. McColl, G. G. Katul, P. Gentine, and D. Entekhabi, Mean-velocity profile of smooth channel flow explained by a cospectral budget model with wall-blockage, Phys. Fluids **28**, 035107 (2016).
[62] W. J. T. Bos, H. Touil, L. Shao, and J. P. Bertoglio, On the behavior of the velocity-scalar cross correlation spectrum in the inertial range, Phys. Fluids **16**, 3818 (2004).
[63] W. J. T. Bos and J. P. Bertoglio, Inertial range scaling of scalar flux spectra in uniformly sheared turbulence, Phys. Fluids **19**, 025104 (2007).
[64] S. Corrsin, Further generalization of Onsager's cascade model for turbulent spectra, Phys. Fluids **7**, 1156 (1964).
[65] L. Onsager, Statistical hydrodynamics, Nuovo Cimento **6**, 279 (1949).

[66] H. Tennekes and J. L. Lumley, *A First Course in Turbulence* (MIT Press, Cambridge, MA, 1972).
[67] A. A. M. Holtslag and C. H. Moeng, Eddy diffusivity and countergradient transport in the convective atmospheric boundary layer, J. Atmos. Sci. **48**, 1690 (1991).
[68] A. N. Kolmogorov, The local structure of turbulence in incompressible viscous fluid for very large Reynolds number, Dokl. Akad. Nauk SSSR **30**, 301 (1941).
[69] H. Liu, Y. Zhang, S. Liu, H. Jiang, L. Sheng, and Q. L. Williams, Eddy covariance measurements of surface energy budget and evaporation in a cool season over southern open water in mississippi, J. Geophys. Res. Atmos. **114**, D04110 (2009).
[70] H. Liu, Q. Zhang, G. G. Katul, J. J. Cole, F. S. Chapin, III, and S. MacIntyre, Large CO_2 effluxes at night and during synoptic weather events significantly contribute to CO_2 emissions from a reservoir, Environ. Res. Lett. **11**, 064001 (2016).
[71] U. Frisch, in *Turbulence: The Legacy of A. N. Kolmogorov* (Cambridge University Press, New York, 1995), p. 296.
[72] J. D. Wilson, Monin-Obukhov functions for standard deviations of velocity, Boundary-Layer Meteorol. **129**, 353 (2008).
[73] C. I. Hsieh and G. G. Katul, Dissipation methods, Taylor's hypothesis, and stability correction functions in the atmospheric surface layer, J. Geophys. Res. Atmos. **102**, 16391 (1997).
[74] K. R. Sreenivasan and R. A. Antonia, The phenomenology of small scale turbulence, Annu. Rev. Fluid Mech. **29**, 435 (1997).
[75] S. Corrsin, On the spectrum of isotropic temperature fluctuations in isotropic turbulence, J. Appl. Phys. **22**, 469 (1951).
[76] Z. Warhaft, Passive scalars in turbulent flows, Annu. Rev. Fluid Mech. **32**, 203 (2000).
[77] P. K. Yeung, S. Xu, and K. R. Sreenivasan, Schmidt number effects on turbulent transport with uniform mean scalar gradient, Phys. Fluids **14**, 4178 (2002).
[78] J. L. Lumley, Similarity and the turbulent energy spectrum, Phys. Fluids **10**, 855 (1967).
[79] S. G. Saddoughi and S. V. Veeravalli, Local isotropy in turbulent boundary layers at high Reynolds number, J. Fluid Mech. **268**, 333 (1994).
[80] T. Ishihara, K. Yoshida, and Y. Kaneda, Anisotropic velocity correlation spectrum at small scales in a homogeneous turbulent shear flow, Phys. Rev. Lett. **88**, 154501 (2002).
[81] G. G. Katul, C. Manes, A. Porporato, E. Bou-Zeid, and M. Chamecki, Bottlenecks in turbulent kinetic energy spectra predicted from structure function inflections using the von Kármán–Howarth equation, Phys. Rev. E **92**, 033009 (2015).
[82] E. Ohtaki, On the similarity in atmospheric fluctuations of carbon dioxide, water vapor, and temperature over vegetated fields, Boundary-Layer Meteorol. **32**, 25 (1985).
[83] D. Li, G. G. Katul, and P. Gentine, The k^{-1} scaling of air temperature spectra in atmospheric surface layer flows, Quart. J. Royal Meteorol. Soc. **142**, 496 (2016).
[84] S. S. Zilitinkevich, On the determination of the height of the Ekman boundary layer, Boundary-Layer Meteorol. **3**, 141 (1972).